Bioorganic & Medicinal Chemistry 21 (2013) 3356–3362

Contents lists available at SciVerse ScienceDirect

Bioorganic & Medicinal Chemistry

journal homepage: www.elsevier.com/locate/bmc

Synthesis and biological evaluation of novel styryl benzimidazole derivatives as probes for imaging of neurofibrillary tangles in Alzheimer's disease

Kenji Matsumura [a], Masahiro Ono [a,*], Masashi Yoshimura [a], Hiroyuki Kimura [a], Hiroyuki Watanabe [a], Yoko Okamoto [b], Masafumi Ihara [b], Ryosuke Takahashi [b], Hideo Saji [a]

[a] Department of Patho-Functional Bioanalysis, Graduate School of Pharmaceutical Sciences, Kyoto University, 46-29 Yoshida Shimoadachi-cho, Sakyo-ku, Kyoto 606-8501, Japan
[b] Department of Neurology, Graduate School of Medicine, Kyoto University, 54 Shogoin Kawahara-cho, Sakyo-ku, Kyoto 606-8507, Japan

ARTICLE INFO

Article history:
Received 9 January 2013
Revised 14 February 2013
Accepted 15 February 2013
Available online 29 March 2013

Keywords:
Alzheimer's disease
Neurofibrillary tangles
Tau
Imaging
Styryl benzimidazole

ABSTRACT

This paper describes the synthesis and biological evaluation of styrylbenzimidazole (SBIM) derivatives as agents for imaging neurofibrillary tangles (NFT) in patients with Alzheimer's disease (AD). SBIM derivatives were prepared with 4-iodobenzene-1,2-diamine and substituted cinnamaldehydes. In binding experiments using recombinant tau and $A\beta_{1-42}$ aggregates, **SBIM-3** showed higher affinity for the tau aggregates than $A\beta_{1-42}$ aggregates (ratio of K_d values was 2.73). In in vitro autoradiography and fluorescent staining, [^{125}I]**SBIM-3** (or **SBIM-3**) bound NFT in sections of AD brain tissue. In biodistribution experiments using normal mice, all [^{125}I]SBIM derivatives showed high initial uptake into (3.20–4.11%ID/g at 2 min after the injection) and rapid clearance from (0.12–0.33%ID/g at 60 min after the injection) the brain. In conclusion, appropriate structural modifications of SBIM derivatives could lead to more useful agents for the in vivo imaging of NFT in AD brains.

© 2013 Elsevier Ltd. All rights reserved.

1. Introduction

Alzheimer's disease (AD), the most common neurodegenerative disorder, is characterized by memory loss and language impairment and its prevalence is increasing together with life expectancy. Although the etiology of AD is not completely understood, the progressive accumulation of senile plaques (SP) composed of amyloid β (Aβ) peptide and neurofibrillary tangles (NFT) composed of hyperphosphorylated tau protein are two neuropathological hallmarks of the disease.[1] Currently, a post-mortem histopathological examination of SP and NFT is the only way to confirm AD. Since these markers probably appear many years prior to the cognitive symptoms of AD,[2,3] detecting SP and/or NFT in vivo may lead to an early diagnosis. Additionally, monitoring these targets in vivo may also support the development of new medical techniques such as immunotherapy.

Positron emission tomography (PET) and single photon emission computed tomography (SPECT) are useful for imaging SP and/or NFT noninvasively in living brain tissue. Since deposits of SP have been demonstrated at the earliest stages of the disease process, PET/SPECT imaging agents targeting SP such as [^{11}C]SB-13,[4,5] [^{11}C]PIB,[6,7] [^{11}C]BF-227,[8] [^{18}F]FDDNP,[9,10] [^{18}F]BAY94-9172,[11,12] [^{18}F]AV-45,[13,14] [^{123}I]IMPY[15] have been developed and succeeded in imaging SP in AD brains. Among these compounds, [^{11}C]PIB has been used in thousands of clinical studies and proved its utility.[6,16] However, a positive [^{11}C]PIB scan identifies the presence of SP in nearly all AD patients, 60% of individuals with mild cognitive impairment (MCI), and 20–30% of cognitively normal elderly subjects,[17] indicating that SP deposit not only in AD brains but also in healthy brains with age.

The accumulation of NFT corresponds with the severity of clinical symptoms of AD.[18–20] There are several PET/SPECT imaging agents targeting NFT such as [^{11}C]BF-158,[21] [^{18}F]THK-523,[22] [^{125}I]TH2,[23] [^{125}I]PDB-3,[24] [^{18}F]FPPDB,[25] and [^{18}F]T808.[26] In in vitro experiments, these agents have exhibited higher affinity for tau than Aβ. For example, autoradiographic analysis using AD brain sections showed that positive [^{18}F]THK-523-binding corresponded with the accumulation of NFT. Although [^{18}F]THK-523 has been investigated clinically so far, its accumulation in the white matter of the brain suggests interference with specific imaging.[27] Therefore, further research into the development of NFT-specific tracers is needed.

We recently developed radioiodinated compounds based on a phenyldiazenylbenzothiazole (PDB) scaffold as NFT imaging agents. In in vitro autoradiographic and fluorescent staining experiments, [^{125}I]PDB-3 (or PDB-3) bound to NFT in AD brain sections.[24] However, PDB derivatives showed low uptake into (0.94–1.03%ID/g at 2 min after the injection) and persistent localization in normal

* Corresponding author. Tel.: +81 75 753 4608; fax: +81 75 753 4568.
E-mail address: ono@pharm.kyoto-u.ac.jp (M. Ono).

0968-0896/$ - see front matter © 2013 Elsevier Ltd. All rights reserved.
http://dx.doi.org/10.1016/j.bmc.2013.02.054

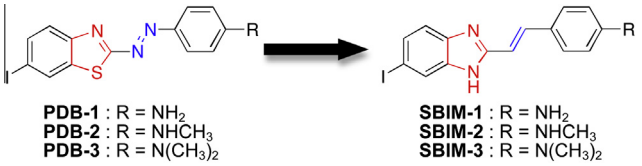

Figure 1. Structures of PDB derivatives and SBIM derivatives.

mouse brains (2.89–3.23%ID/g at 60 min after the injection), which might lead to a low signal-to-noise ratio in AD brains. This nonspecific binding to normal areas in the brains may be due to the high lipophilicity of PDB derivatives.[28] Consequently, we planned to replace the benzothiazole scaffold in PDB with a benzimidazole scaffold with less lipophilicity. Furthermore, we changed the diazo moiety to a styryl moiety since the diazo moiety of PDB derivatives is typically thought to be toxic in humans.[29] Based on this knowledge, we designed styrylbenzimidazole derivatives with less lipophilicity and less toxicity as candidates for in vivo imaging of NFT in AD brains (Fig. 1).

In this study, we synthesized three styrylbenzimidazole (SBIM) derivatives and evaluated their utility as NFT imaging agents. To our knowledge, this is the first time radioiodinated styrylbenzimidazole derivatives have been used as NFT imaging agents.

2. Results and discussion

2.1. Chemistry and radiolabeling

The synthesis of SBIM derivatives was carried out according to Schemes 1A, B, and C. Compounds **1**, **2c**, **3**, and **4c** were obtained by intermolecular cyclization between 4-bromobenzene-1,2-diamine or 4-iodobenzene-1,2-diamine and substituted cinnamaldehydes using $Na_2S_2O_5$ as an oxidant agent (yield, 67.1–86.7%). The monomethyl amino derivatives, **2b** and **4b**, were produced by first reducing the nitro group to an amino group with powdered iron, and subsequent monomethylation of the amino group using paraformaldehyde, sodium borohydride, and sodium methoxide (yield, 69.8–76.5%). Compounds **5a**, **5b**, and **5c** were obtained by protecting the aminogroups of **4a**, **4b**, and **4c** with a *tert*-butoxycarbonyl (Boc) group (yield, 79.4–88.3%). The tributyltin precursors (**6a**, **6b**, and **6c**) were prepared from corresponding bromo compounds using a bromo to tributhyltin exchange reaction catalyzed by $Pd(Ph_3P)_4$ (yield, 30.3–59.0%). The radioiodinated ligands, [^{125}I]**2a** ([^{125}I]**SBIM-1**), [^{125}I]**2b** ([^{125}I]**SBIM-2**), and [^{125}I]**2c** ([^{125}I]**SBIM-3**) were prepared from corresponding tributyltin precursors through an iododestannylation reaction using hydrogen peroxide as an oxidant followed by stirring with TFA to remove the Boc protecting groups with a radiochemical yield of 24.0–45.0%. After purification by HPLC, the specific activity of the no-carrier-added preparation was comparable to that of [^{125}I]NaI, 81.4 TBq/mmol. Finally, the identity of [^{125}I]**2a** ([^{125}I]**SBIM-1**), [^{125}I]**2b** ([^{125}I]**SBIM-2**), and [^{125}I]**2c** ([^{125}I]**SBIM-3**) was verified by coinjection with a nonradioactive compound from HPLC data. HPLC analysis suggested that these derivatives existed as tautomers. All [^{125}I]SBIM derivatives were obtained with radiochemical purity of >99% after purification by HPLC.

2.2. Binding assay with SBIM derivatives using recombinant tau and $A\beta_{1-42}$ aggregates

To quantify the affinity for NFT, we carried out binding experiments using recombinant tau aggregates (Table 1). The fluorescent

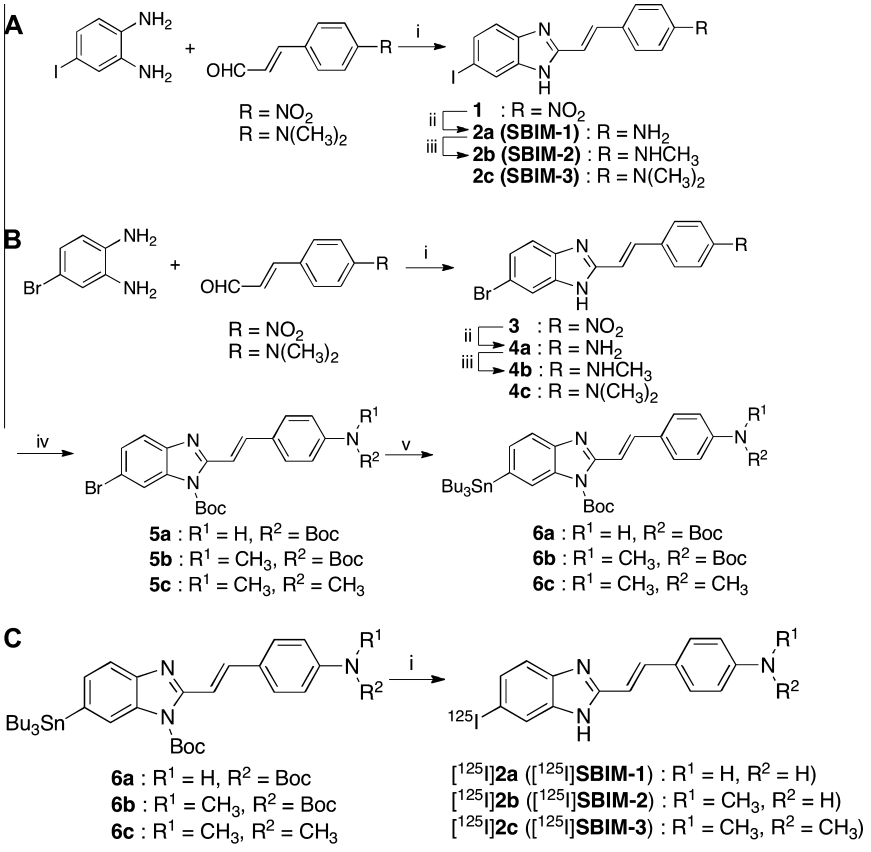

Scheme 1. (A) Reagents and conditions: (i) $Na_2S_2O_5$, DMF, 105 °C; (ii) powdered iron, HCl, 80% EtOH, 90 °C; (iii) NaOMe, $(HCHO)_n$, $NaBH_4$, MeOH, 75 °C. (B) Reagents and conditions: (i) $Na_2S_2O_5$, DMF, 105 °C; (ii) powdered iron, HCl, 80% EtOH, 90 °C; (iii) NaOMe, $(HCHO)_n$, $NaBH_4$, MeOH, 75 °C; (iv) $(Boc)_2O$, guanidine hydrochloride, EtOH, 40 °C; (v) $(Bu_3Sn)_2$, $(Ph_3P)_4Pd$, Et_3N, dioxane, 95 °C. (C) Reagents and conditions: (i) (1) [^{125}I]NaI, 3% H_2O_2, 1 N HCl, rt, (2) TFA, rt.

Table 1
K_d Values of SBIM derivatives for recombinant tau and $A\beta_{1-42}$ aggregates

Compound	K_d[a] (μM)		K_d Ratios of $A\beta_{1-42}$/tau
	Tau	$A\beta_{1-42}$	
SBIM-1	2.36 ± 0.09	0.90 ± 0.27	0.38
SBIM-2	0.45 ± 0.08	0.42 ± 0.05	0.93
SBIM-3	0.30 ± 0.02	0.82 ± 0.10	2.73

[a] Values are the mean ± standard error of the mean for six independent experiments.

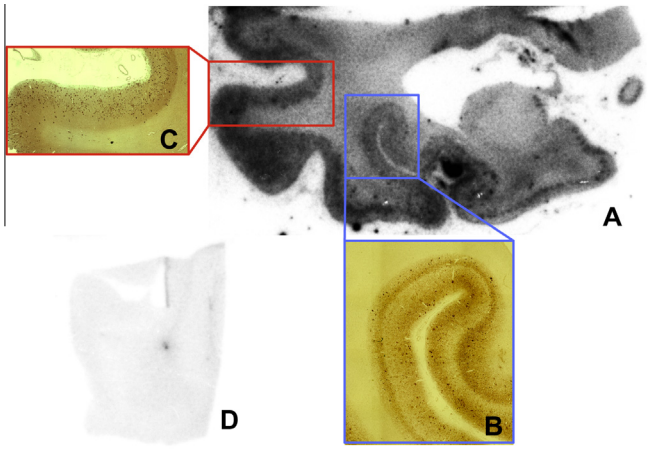

Figure 2. Autoradiogram of [^{125}I]**SBIM-3** in an AD brain section (A) and immunohistochemical staining with an antibody against phosphorylated tau (AT8: B) and $A\beta_{1-42}$ (BC05: C) in adjacent brain sections of A. Autoradiogram of [^{125}I]**SBIM-3** in a control brain section (D).

intensity of SBIM derivatives increased in the presence of tau aggregates. We calculated the apparent binding dissociation constant (K_d) by utilizing this property of SBIM derivatives. The saturation curves of fluorescent intensity revealed the apparent K_d values of **SBIM-1**, **2**, and **3** for tau aggregates to be 2.36, 0.45, and 0.30 μM, respectively. We assumed that SBIM derivatives possibly bind to $A\beta_{1-42}$ aggregates as well as tau aggregates since $A\beta_{1-42}$ aggregates also form a β-sheet structure. Then we carried out the same experiment using $A\beta_{1-42}$ aggregates to evaluate the selective binding affinity between tu and $A\beta_{1-42}$ aggregates. The apparent K_d values of **SBIM-1**, **2**, and **3** for $A\beta_{1-42}$ aggregates were 0.90, 0.42, and 0.82 μM, respectively. The ratios of apparent K_d values of SBIM derivatives were 0.38, 0.93, and 2.73, respectively. Although **SBIM-1** and **SBIM-2** had lower affinity for tau aggregates than $A\beta_{1-42}$ aggregates, **SBIM-3** had higher affinity for tau aggregates than $A\beta_{1-42}$ aggregates. These results suggested that minor changes of substituted groups in the SBIM scaffold might influence the selective binding between tau and $A\beta_{1-42}$ aggregates. Therefore, further appropriate modification of SBIM derivatives may lead to useful agents with much higher affinity for NFT than SP.

2.3. In vitro autoradiography

[^{125}I]**SBIM-3**, which showed the best ratio of K_d values for tau aggregates to $A\beta_{1-42}$ aggregates, was investigated for its binding to NFT by in vitro autoradiography in an AD brain section. The autoradiographic image showed a remarkable accumulation of radioactivity in gray matter (Fig. 2A). The level of radioactivity in white matter was relatively low, indicating the nonspecific binding of [^{125}I]**SBIM-3** in the AD brain section to be low. [^{125}I]**SBIM-3** showed almost no accumulation in the control brain section (Fig. 2D). The accumulation of radioactivity in the AD brain section corresponded with the results of immunohistochemical staining with both the anti phosphorylated tau antibody (AT8) and the anti $A\beta_{1-42}$ antibody (BC05) (Fig. 2B and C, respectively). Compared with the results of immunohistochemical staining, [^{125}I]**SBIM-3** bound both NFT and SP, which reflected **SBIM-3**'s relatively low selective affinity (the ratio of K_d values of **SBIM-3** is 2.73). To achieve high contrast between NFT and SP, it is necessary to develop agents with higher affinity for NFT and lower affinity for SP by introducing another substituted group such as a methoxy group into SBIM derivatives.

2.4. Fluorescent staining of AD brain sections

To further confirm the affinity of **SBIM-3** for NFT in the AD brain, a fluorescent staining experiment was carried out in the brain sections of the same AD patient (Fig. 3A). A number of fluorescent spots were clearly stained in the entorhinal cortex. Then, the same patient's brain section was stained by Thioflavin S (ThS) (Fig. 3B). The fluorescent spots obtained with ThS corresponded to the spots obtained with **SBIM-3**, suggesting that **SBIM-3** bound to NFT in the AD brain section.

2.5. In vivo biodistribution in normal mice

To evaluate the uptake of SBIM derivatives into brains, a biodistribution study in normal mice was performed with [^{125}I]**SBIM-1**,

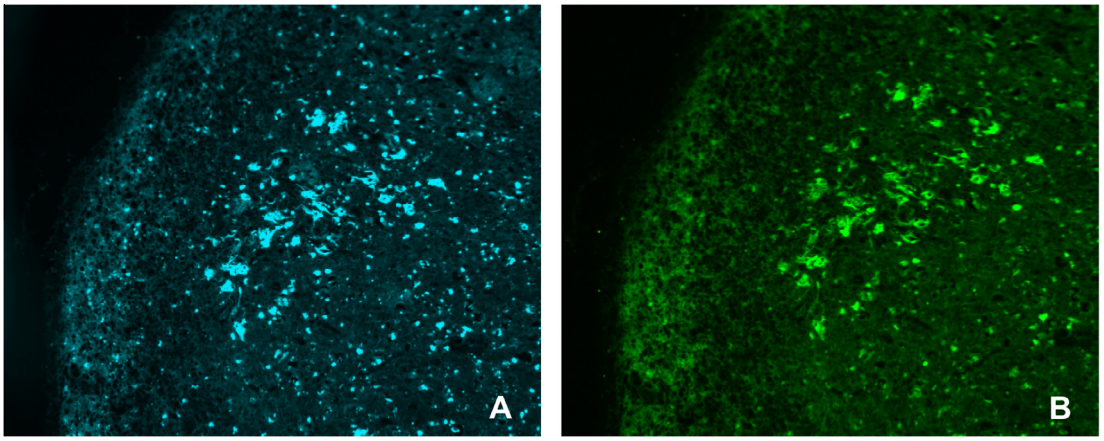

Figure 3. Fluorescent staining of the AD brain sections (entorhinal cortex) using SBIM-3 (A) and ThS (B).

Table 2
Biodistribution of radioactivity after injection of SBIM derivatives in normal mice[a]

Tissue	Time after injection (min)			
	2	10	30	60
***[^{125}I]2a* (*[^{125}I]SBIM-1*)**				
Blood	5.94 (0.34)	2.72 (0.72)	1.57 (0.41)	1.24 (0.22)
Liver	29.4 (5.46)	29.9 (2.52)	19.3 (1.18)	15.6 (2.38)
Kidney	10.6 (1.36)	5.04 (0.38)	2.54 (0.38)	3.25 (1.63)
Intestine	4.09 (0.55)	13.7 (2.43)	22.1 (3.36)	27.4 (5.55)
Spleen	5.50 (1.46)	4.87 (0.89)	2.71 (0.27)	2.46 (0.53)
Pancreas	4.99 (1.25)	1.93 (0.48)	0.69 (0.13)	1.43 (2.11)
Heart	8.31 (1.12)	2.84 (0.33)	1.48 (0.17)	1.13 (0.29)
Lung	9.09 (2.74)	3.55 (0.37)	1.62 (0.26)	1.44 (0.14)
Stomach[b]	1.70 (0.25)	4.13 (1.07)	3.60 (0.88)	4.37 (1.54)
Brain	3.20 (0.31)	1.40 (0.22)	0.26 (0.02)	0.12 (0.03)
***[^{125}I]2b* (*[^{125}I]SBIM-2*)**				
Blood	3.65 (0.54)	2.76 (0.43)	2.19 (0.33)	1.37 (0.31)
Liver	19.9 (1.97)	23.2 (1.97)	16.0 (2.38)	11.0 (2.05)
Kidney	11.2 (1.24)	5.85 (1.26)	3.07 (0.54)	2.02 (0.65)
Intestine	4.96 (1.18)	11.5 (2.17)	28.4 (5.49)	30.0 (7.54)
Spleen	5.19 (0.36)	4.90 (0.51)	3.13 (0.99)	1.74 (0.37)
Pancreas	6.80 (2.51)	2.58 (0.11)	0.92 (0.14)	0.51 (0.08)
Heart	6.68 (0.53)	2.80 (0.14)	1.28 (0.15)	0.74 (0.14)
Lung	7.13 (1.17)	3.55 (0.30)	1.93 (0.27)	1.32 (0.18)
Stomach[b]	2.31 (0.68)	4.88 (2.31)	4.65 (1.48)	2.97 (1.03)
Brain	4.11 (0.37)	1.42 (0.08)	0.36 (0.05)	0.14 (0.02)
***[^{125}I]2c* (*[^{125}I]SBIM-3*)**				
Blood	3.83 (0.34)	3.24 (0.30)	1.88 (0.23)	1.28 (0.29)
Liver	17.4 (1.18)	19.2 (1.48)	14.9 (3.19)	10.1 (0.98)
Kidney	11.7 (0.87)	7.28 (0.57)	4.32 (0.73)	2.26 (0.28)
Intestine	3.11 (0.56)	9.22 (1.66)	18.2 (3.12)	26.5 (6.59)
Spleen	3.48 (0.71)	3.69 (0.78)	2.66 (0.65)	1.42 (0.43)
Pancreas	5.40 (1.57)	3.31 (0.35)	1.67 (0.25)	0.89 (0.13)
Heart	8.56 (0.92)	3.46 (0.34)	2.00 (0.28)	1.12 (0.21)
Lung	7.39 (0.34)	3.98 (0.22)	2.20 (0.32)	1.39 (0.22)
Stomach[b]	1.67 (0.25)	2.82 (0.87)	3.83 (0.86)	3.56 (1.49)
Brain	3.28 (0.25)	1.61 (0.18)	0.68 (0.11)	0.33 (0.06)

[a] Each value represents the mean (SD) for 5 animals.
[b] Expressed as % injected dose per organ.

2, and **3** (Table 2). The uptake of [^{125}I]**SBIM-1**, **2**, and **3** into brains at 2 min after the injection ($brain_{2\ min}$) was 3.20%, 4.11%, and 3.28%ID/g, respectively. Since there are neither NFT nor SP in normal brains, the injected agents should washout rapidly. All [^{125}I]SBIM derivatives showed a rapid clearance from the brain ($brain_{60\ min}$ of [^{125}I]**SBIM-1**, **2**, and **3** were 0.12%, 0.14%, and 0.33%ID/g, respectively). The $brain_{2\ min}/brain_{60\ min}$ ratio of [^{125}I]**SBIM-1**, **2**, and **3** was 26.7, 29.4, and 9.94, much higher than that of [^{125}I]PDB derivatives (0.30, 0.33, and 0.33 for [^{125}I]**PDB-1**, **2**, and **3**, respectively). Compared to [^{125}I]PDB derivatives, [^{125}I]SBIM derivatives showed much better pharmacokinetics in normal mouse brains (Fig. 4). Moreover, the $brain_{2\ min}/brain_{60\ min}$ ratios of [^{125}I]SBIM derivatives were higher than those of [^{11}C]BF158,[21] [^{18}F]THK-523,[22] [^{125}I]TH2,[23] [^{18}F]FPPDB,[25] and [^{18}F]T808[26] reported previously as NFT imaging agents (5.38, approximate 1.83, 6.16, 1.69 (the ratios of $brain_{2\ min}/brain_{60\ min}$), and 2.92 (the ratios of $brain_{2.5\ min}/brain_{20\ min}$), respectively). The log P values for [^{125}I]**SBIM-1**, **2**, and **3** were 1.88, 2.00, and 2.23, much lower than that for [^{125}I]**PDB-3** (3.84). These results suggest that reducing lipophilicity might lead to better pharmacokinetics of [^{125}I]SBIM derivatives in the brain. The initial uptake was highest in the liver ($liver_{2\ min}$, 17.4–29.4%ID/g) and kidney ($kidney_{2\ min}$, 10.6–11.7%ID/g) followed by a rapid clearance ($liver_{60\ min}$, 10.1–15.6%ID/g and $kidney_{60\ min}$, 2.02–3.25%ID/g), whereas the intestines showed an accumulation of radioactivity over time ($intestine_{60\ min}$ was 26.5–30.0%ID/g). Since the accumulation in the stomach was low (2.97–4.37%ID), all [^{125}I]SBIM derivatives were stable in vivo by 60 min after the injection.

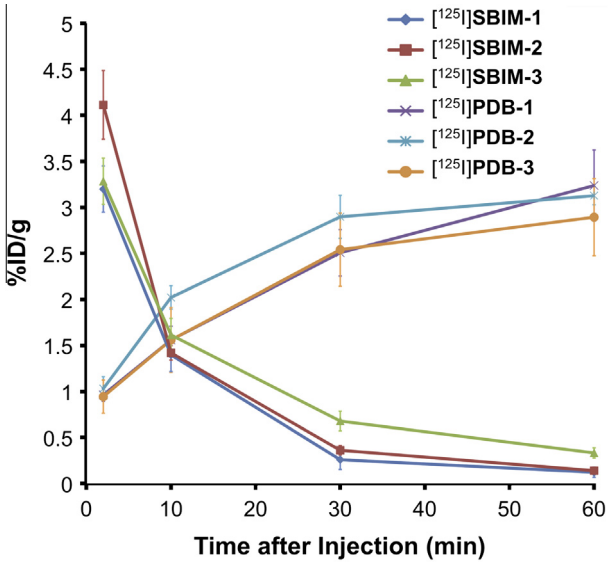

Figure 4. Comparison of brain uptake of [^{125}I]PDB derivatives and [^{125}I]SBIM derivatives.

3. Conclusion

In conclusion, we designed, synthesized, and evaluated a new series of SBIM derivatives as potential NFT imaging agents. In binding experiments, **SBIM-3** showed higher affinity for tau aggregates than $A\beta_{1-42}$ aggregates. In vitro autoradiography and fluorescent staining revealed that NFT were stained with [^{125}I]**SBIM-3** (or **SBIM-3**). In biodistribution experiments using normal mice, all [^{125}I]SBIM derivatives displayed a better initial uptake into and rapid clearance from brains after the injection. The $brain_{2\ min}/brain_{60\ min}$ ratios of [^{125}I]SBIM derivatives were much higher than that of any other NFT imaging agent reported previously, perhaps due to lower lipophilicity. Appropriate structural modifications of SBIM derivatives may lead to more useful agents for the in vivo imaging of NFT in AD brains.

4. Experimental

All reagents were commercial products and used without further purification unless indicated otherwise. ^{1}H NMR spectra were recorded on a JEOL JNM-LM400 with TMS as an internal standard. Coupling constants are reported in Hertz. Multiplicity was defined as singlet (s), doublet (d), triplet (t), and multiplet (m). Mass spectra were obtained on a SHIMADZU LCMS-2010 EV. HPLC was performed with a Shimadzu system (a LC-20AT pump with a SPD-20A UV detector, λ = 254 nm) using a Cosmosil C_{18} column (Nacalai Tesque, 5C_{18}-MS-II, 4.6 × 150 mm) and acetonitrile/water (containing 0.1% Et_3N) = 6/4 or 5/5 as the mobile phase at a flow rate of 1.0 mL/min. All key compounds were proven by this method to show >99% purity.

4.1. Chemistry

4.1.1. (*E*)-6-Iodo-2-(4-nitrostyryl)-1*H*-benzimidazole (1)

A mixture of 4-iodobenzene-1,2-diamine (1.17 g, 5.00 mmol), 4-nitrocinnamaldehyde (886 mg, 5.00 mmol), and $Na_2S_2O_5$ (951 mg, 5.00 mmol) dissolved in 5 mL of dimethylformamide (DMF) was heated to 105 °C and stirred for 2 h. Ice water (50 mL) was added, and the precipitate formed was collected by filtration, washed with water and dried under vacuum to obtain 1.66 g of **1** (85.0%) as a brown solid. (400 MHz, DMSO-d_6) δ 8.25 (d, J = 8.9 Hz, 2H), 7.90–7.93 (m, 3H), 7.78 (d, J = 16.5 Hz, 1H), 7.42–7.50 (m, 3H). MS (APCI) m/z 392 [MH^+].

4.1.2. (*E*)-4-[2-(6-Iodo-1*H*-benzimidazol-2-yl)ethenyl]aniline (2a)

To a mixture of **1** (1.96 g, 5.00 mmol) and concentrated HCl (1.20 mL) in 80% EtOH (60 mL) was added powdered iron (1.12 g, 20.0 mmol). The reaction mixture was stirred for 24 h under reflux, and then cooled to room temperature. The precipitate of iron oxides and hydroxy salts was removed by filtration. The solvent was removed and the residue was neutralized with saturated $NaHCO_3$(aq) and extracted with ethyl acetate. The organic phase was dried over Na_2SO_4 and filtered. The filtrate was concentrated and the residue was purified by silica gel chromatography (chloroform/methanol = 10/1) to give 1.53 g of **2a** (84.6%) as a yellow solid. mp: 116–118 °C ^{1}H NMR (400 MHz, CD_3OD) δ 7.80 (s, 1H), 7.44 (d, J = 16.6 Hz, 1H), 7.40 (dd, J = 1.6, 8.4 Hz, 1H), 7.31 (d, J = 8.4 Hz, 2H) 7.22 (d, J = 8.4 Hz, 1H), 6.78 (d, J = 16.5 Hz, 1H), 6.68 (d, J = 8.4 Hz, 2H). HRMS (EI) m/z calcd for $C_{15}H_{12}IN_3$ (M^+) 361.0076, found 361.0080.

4.1.3. (*E*)-4-[2-(6-Iodo-1*H*-benzimidazol-2-yl)ethenyl]-*N*-methylaniline (2b)

A solution of NaOMe (28 wt % in MeOH, 3.67 mL) was added to a mixture of **2a** (1.65 g, 4.58 mmol) and paraformaldehyde (741 mg, 24.7 mmol) in methanol (20 mL) dropwise. The mixture was stirred under reflux for 1 h. After $NaBH_4$ (866 mg, 22.9 mmol) was added, the solution was heated under reflux for 2 h. 1 M NaOH (30 mL) was added to the cold mixture and extracted with ethyl acetate. The organic phase was dried over Na_2SO_4 and filtered. The solvent was removed, and the residue was purified by silica gel chromatography (chloroform/methanol = 49/1) to give 1.20 g of **2b** (69.8%) as a yellow solid. mp: 117-119 °C ^{1}H NMR (400 MHz, CD_3OD) δ 7.75 (s, 1H), 7.41 (d, J = 16.3 Hz, 1H), 7.39 (dd, J = 1.7, 8.4 Hz, 1H), 7.31 (d, J = 8.7 Hz, 2H), 7.20 (d, J = 8.4 Hz, 1H), 6.73 (d, J = 16.3 Hz, 1H), 6.52 (d, J = 8.7 Hz, 2H), 2.73 (s, 3H). HRMS (EI) m/z calcd for $C_{16}H_{14}IN_3$ (M^+) 375.0233, found 375.0235.

4.1.4. (*E*)-4-[2-(6-Iodo-1*H*-benzimidazol-2-yl)ethenyl]-*N*,*N*-dimethylaniline (2c)

The same reaction described above to prepare **1** was used, and 320 mg of **2c** was obtained in a yield of 82.3% as a yellow solid from 4-iodobenzene-1,2-diamine and 4-dimethylaminocinnamaldehyde. mp: 245 °C (decomposition) ^{1}H NMR (400 MHz, DMSO-d_6) δ 7.82 (s, 1H), 7.56 (d, J = 16.2 Hz, 1H), 7.49 (d, J = 9.0 Hz, 2H), 7.41 (dd, J = 1.7, 8.4 Hz, 1H), 7.32 (d, J = 8.1 Hz, 1H), 6.90 (d, J = 16.5 Hz, 1H), 6.75 (d, J = 8.7 Hz, 2H), 2.97(s, 6H). HRMS (EI) m/z calcd for $C_{17}H_{16}IN_3$ (M^+) 389.0389, found 389.0386.

4.1.5. (*E*)-6-Bromo-2-(4-nitrostyryl)-1*H*-benzimidazole (3)

The same reaction described above to prepare **1** was used, and 921 mg of **3** was obtained in a yield of 67.1% as a yellow solid from 4-bromo-1,2-diaminobenzene and 4-nitrocinnamaldehyde. ^{1}H NMR (400 MHz, DMSO-d_6) δ 8.27 (d, J = 7.3 Hz, 2H), 7.95 (d, J = 7.8 Hz, 2H), 7.78–7.82 (m, 2H), 7.54 (d, J = 8.2 Hz, 1H), 7.45 (d, J = 16.5 Hz, 1H), 7.35 (d, J = 8.7 Hz, 1H), MS (APCI) m/z 344 [MH^+].

4.1.6. (*E*)-4-[2-(6-Bromo-1*H*-benzimidazol-2-yl)ethenyl]aniline (4a)

The same reaction described above to prepare **2a** was used, and 545 mg of **4a** was obtained in a yield of 81.0% as a yellow solid from **3**. ^{1}H NMR (400 MHz, CD_3OD) δ 7.65 (s, 1H), 7.52 (d, J = 16.5 Hz, 1H), 7.41 (d, J = 8.5 Hz, 1H), 7.38 (d, J = 8.4 Hz, 2H), 7.32 (dd, J = 1.8, 8.5 Hz, 1H), 6.85 (d, J = 16.4 Hz, 1H), 6.71 (d, J = 8.5 Hz, 2H). MS (APCI) m/z 314 [MH^+].

4.1.7. (*E*)-4-[2-(6-Bromo-1*H*-benzimidazol-2-yl)ethenyl]-*N*-methylaniline (4b)

The same reaction described above to prepare **2b** was used, and 500 mg of **4b** was obtained in a yield of 76.5% as a yellow solid from **4a**. ^{1}H NMR (400 MHz, CD_3OD) δ 7.84 (s, 1H), 7.59 (s, 1H), 7.44 (d, J = 16.3 Hz, 1H), 7.31–7.34 (m, 3H), 7.24 (dd, J = 1.8, 8.5 Hz, 1H), 6.75 (d, J = 16.5 Hz, 1H), 6.53 (d, J = 8.7 Hz, 2H), 2.76 (s, 3H). MS (APCI) m/z 328 [MH^+].

4.1.8. (*E*)-4-[2-(6-Bromo-1*H*-benzimidazol-2-yl)ethenyl]-*N*,*N*-dimethylaniline (4c)

The same reaction described above to prepare **1** was used, and 340 mg of **4c** was obtained in a yield of 86.7% as a yellow solid from 4-bromo-1,2-diaminobenzene and 4-dimethylaminocinnamaldehyde. ^{1}H NMR (400 MHz, CD_3OD) δ 7.62 (s, 1H), 7.51 (d, J = 16.5 Hz, 1H), 7.45 (d, J = 8.9 Hz, 2H), 7.39 (d, J = 8.5 Hz, 1H), 7.29 (dd, J = 1.8, 8.5 Hz, 1H), 6.84 (d, J = 16.4 Hz, 1H), 6.74 (d, J = 8.9 Hz, 2H), 2.99 (s, 6H). MS (APCI) m/z 342 [MH^+].

4.1.9. (*E*)-4-[2-(6-Bromo-1-*tert*-butoxycarbonyl-benzimidazo-2-yl)ethenyl]-*N*-*tert*-butoxycarbonylaniline (5a)

Compound **4a** (682 mg, 2.00 mmol) was added to a stirred solution of guanidine hydrochloride (15 mol %) and $(Boc)_2O$ (437 mg, 2.00 mmol) in EtOH (5 mL), at 40 °C and stirred for 2 h. The solvent was removed and extracted with ethyl acetate. The organic phase was dried over Na_2SO_4 and filtered. The solvent was removed, and the residue was purified by silica gel chromatography (ethyl acetate/hexane = 1/4) to give 700 mg of **5a** (79.4%) as a yellow solid. ^{1}H NMR (400 MHz, $CDCL_3$) δ 8.12 (s, 1H), 7.92 (d, J = 16.0 Hz, 1H), 7.78–7.84 (m, 2H), 7.56 (d, J = 8.7 Hz, 2H), 7.39–7.45 (m, 3H), 1.75 (s, 9H), 1.57 (s, 9H). MS (APCI) m/z 514 [MH^+].

4.1.10. (*E*)-4-[2-(6-Bromo-1-*tert*-butoxycarbonyl-benzimidazo-2-yl)ethenyl]-*N*-*tert*-butoxycarbonyl-*N*-methylaniline (5b)

The same reaction described above to prepare **5a** was used, and 1.50 g of **5b** was obtained in a yield of 81.3% as a yellow solid from **4b**. ^{1}H NMR (400 MHz, acetone-d_6) δ 7.91–7.92 (m, 2H), 7.67 (d, J = 8.5 Hz, 2H), 7.58–7.60 (m, 1H), 7.48–7.51 (m, 1H), 7.41 (d, J = 8.5 Hz, 2H), 7.20–7.31 (m, 1H), 3.28 (s, 3H), 1.78–1.80 (m, 9H), 1.48 (s, 9H) MS (APCI) m/z 528 [MH^+].

4.1.11. (*E*)-4-[2-(6-Bromo-1-*tert*-butoxycarbonyl-benzimidazo-2-yl)ethenyl]-*N*,*N*-dimethylaniline (5c)

The same reaction described above to prepare **5a** was used, and 150 mg of **5c** was obtained in a yield of 88.3% as a yellow solid from **4c**. ^{1}H NMR (400 MHz, $CDCL_3$) δ 8.10 (s, 1H) 7.93 (d, J = 15.9 Hz, 1H), 7.67 (d, J = 15.9 Hz, 1H), 7.51–7.55 (m, 3H), 7.42 (dd, J = 1.8, 8.5 Hz, 1H), 6.70 (d, J = 8.8 Hz, 2H), 3.02 (s, 6H), 1.76 (s, 9H). MS (APCI) m/z 442 [MH^+].

4.1.12. (*E*)-4-[2-(1-*tert*-Butoxycarbonyl-6-tributylstannyl-benzimidazo-2-yl)ethenyl]-*N*-*tert*-butoxycarbonylaniline (6a)

A mixture of **5a** (494 mg, 1.10 mmol), bis(tributyltin) (1.12 mL, 2.20 mmol), and $(Ph_3P)_4Pd$ (555 mg, 0.480 mmol) in a mixed solvent (15 mL, dioxane/Et_3N = 2/1) was stirred under reflux for 5 h. The solvent was removed, and the residue was purified by silica gel chromatography (hexane/ethyl acetate = 4/1) to give 432 mg of **6a** (59.0%) as a yellow oil. ^{1}H NMR (400 MHz, $CDCL_3$) δ 7.93 (d, J = 16.0 Hz, 1H) 7.83–7.90 (m, 3H), 7.56 (d, J = 8.7 Hz, 2H), 7.37–7.41 (m, 3H), 6.70 (s,1H), 1.75 (s, 9H), 1.52 (s, 9H), 0.87–1.66 (m, 27H). MS (APCI) m/z 726 [MH^+].

4.1.13. (*E*)-4-[2-(1-*tert*-Butoxycarbonyl-6-tributylstannyl-benzimidazo-2-yl)ethenyl]-*N*-*tert*-butoxycarbonyl-*N*-methylaniline (6b)

The same reaction described above to prepare **6a** was used, and 210 mg of **6b** was obtained in a yield of 30.3% as a yellow oil from **5b**. ^{1}H NMR (400 MHz, CD_3OD) δ 7.78–7.84 (m, 2H), 7.66–7.71 (m, 2H), 7.51 (d, J = 8.7 Hz, 2H), 7.30 (d, J = 8.1 Hz, 1H), 7.21 (d,

J = 8.5 Hz, 2H), 3.16 (s, 3H), 1.66 (s, 9H), 1.37 (s, 9H), 0.78–1.59 (m, 27H). MS (APCI) m/z 740 [MH^+].

4.1.14. (*E*)-4-[2-(1-*tert*-Butoxycarbonyl-6-tributylstannyl-benzimidazo-2-yl)ethenyl]-*N*,*N*-dimethylaniline (6c)

The same reaction described above to prepare **6a** was used, and 210 mg of **6c** was obtained in a yield of 40.3% as a yellow oil from **5c**. ^{1}H NMR (400 MHz, $CDCL_3$) δ 7.94 (d, J = 16.0 Hz, 1H), 7.87 (d, J = 7.9 Hz, 1H), 7.83 (s, 1H) 7.74 (d, J = 15.9 Hz, 1H), 7.53 (d, J = 8.5 Hz, 2H), 7.34 (d, J = 8.8 Hz, 1H), 6.70 (d, J = 8.9 Hz, 2H), 3.01 (s, 6H) 1.74 (s, 9H), 0.86–1.67 (m, 27H). MS (APCI) m/z 654 [MH^+].

4.2. Binding assay with SBIM derivatives using recombinant tau and $A\beta_{1-42}$ aggregates

The 441-aa isoform of human tau was expressed from a cDNA clone in *Escherichia coli* and purified as described previously.[30] Tau aggregates were prepared by incubating tau protein (1 mg/mL in MES buffer, pH 6.8) at 37 °C for 3 days with gentle and constant shaking in the presence of 0.1 mg/mL heparin. A solid form of $A\beta_{1-42}$ was purchased from Peptide Institute (Osaka, Japan). Aggregation was achieved by gently dissolving the peptide (0.25 mg/mL) in PBS solution (pH 7.4). The solutions were incubated at 37 °C for 42 h with gentle and constant shaking. The binding experiments were carried out in Protein LoBind Tubes (Eppendorf). A mixture of tau aggregates (final conc. 10 μg/mL) or $A\beta_{1-42}$ aggregates (final conc. 10 μg/mL) were incubated at room temperature for 30 min in the presence of SBIM derivatives (final conc. 0.02–10 μM), dispensed to MULTI WELL PLATE (0.4 mL × 96 wells flatbottom, SUMITOMO BAKELITE CO., LTD, Japan), and subjected to fluorescence spectroscopy (λ_{ex} = 440 nm; λ_{em} = 480 nm for $A\beta_{1-42}$ aggregates and λ_{ex} = 440 nm; λ_{em} = 510 nm for tau aggregates). The fluorescence intensity was plotted and the apparent K_d values of SBIM derivatives for recombinant tau and $A\beta_{1-42}$ aggregates were calculated from the fluorescent saturation curves using GraphPad Prism software (Graph Pad software, San Diego, CA).

4.3. Radiolabeling

The radioiodinated forms of compounds [^{125}I]**2a** ([^{125}I]**SBIM-1**), [^{125}I]**2b** ([^{125}I]**SBIM-2**), and [^{125}I]**2c** ([^{125}I]**SBIM-3**) were prepared from the corresponding tributyltin derivatives by iododestannylation. Briefly, to initiate the reaction, 100 μL of H_2O_2 (3%) was added to a mixture of a tributyltin derivative (150 μg/150 μL EtOH), [^{125}I]NaI (3.7–7.4 MBq, specific activity 81.4 TBq/mmol), and 100 μL of 1 N HCl in a sealed vial. The reaction was allowed to proceed at room temperature for 15 min and terminated by addition of saturated $NaHSO_3$(aq) (200 μL). After neutralization with sodium hydrogen carbonate and extraction with ethyl acetate, the extract was dried by passing through an anhydrous Na_2SO_4 column. TFA (80 μL) was added to the solution and blown dry with a stream of nitrogen gas. The radioiodinated ligand was purified by HPLC on a Cosmosil C_{18} column with an isocratic solvent of acetonitrile/H_2O (containing 0.1% Et_3N) = 6/4 or 5/5 at a flow rate of 1.0 mL/min.

4.4. Measurement of log*P* values

The experimental determination of partition coefficients of [^{125}I]**2a** ([^{125}I]**SBIM-1**), [^{125}I]**2b** ([^{125}I]**SBIM-2**), and [^{125}I]**2c** ([^{125}I]**SBIM-3**) was performed in 1-octanol and PBS (−) at a pH of 7.4. 1-Octanol (3.0 mL) and PBS (−) (3.0 mL) were pipetted into a 12-mL-test tube containing 0.37 MBq of test compounds. The test tube was vortexed for 2 min, and centrifuged (10 min, 2000 rpm). Aliquots (500 μL) from the 1-octanol and PBS (−) phases were transferred into two test tubes for counting. The remainder of the 1-octanol phase was transferred (1 mL) into a new test tube. 1-Octanol (2.0 mL) and PBS (−) (3.0 mL) were pipetted into the test tube. The vortexing, centrifuging, and counting were repeated. The amount of radioactivity in each tube was measured with a γ counter (Perkin Elmer, Wizard 1470). The partition coefficient was calculated using Eq. 1:

$$(\text{counts}/\mu\text{L in 1-octanol})/(\text{counts}/\mu\text{L in buffer}) = r \quad (1)$$

4.5. In vitro autoradiography

Postmortem brain tissues from an autopsy-confirmed case of AD (a 93-year-old, female) and a control (a 73-year-old, female) were obtained from the Graduate School of Medicine, Kyoto University and BioChain Institute Inc., respectively. The presence and location of NFT and SP in the sections were confirmed with immunohistochemical staining using anti-phosphoylated tau antibody (AT8) and $A\beta_{1-42}$ antibody (BC05), respectively. Six-micrometer-thick serial sections of paraffin-embedded blocks were used for staining. The sections were subjected to two 15-min incubations in xylene, two 1-min incubations in 100% EtOH, one 1-min incubation in 90% EtOH, one 1-min incubation in 80% EtOH, and one 1-min incubation in 70% EtOH to completely deparaffinize them, followed by two 2.5-min washes in water. The sections were incubated with [^{125}I]**2c** ([^{125}I]**SBIM-3**) (92.5 kBq/100 μL) for 1 h at room temperature. They were then dipped in 50% EtOH for 2 h and washed with water for 30 s. After drying, the ^{125}I-labeled sections were exposed to a BAS imaging plate (Fuji Film, Tokyo, Japan) overnight. Autoradiographic images were obtained using a BAS5000 scanner system (Fuji Film).

4.6. Immunohistochemical staining of NFT and SP in human AD brain sections

Postmortem brain tissues from an autopsy-confirmed case of AD (a 93-year-old, female) were obtained from the Graduate School of Medicine, Kyoto University. Deparaffinization was carried out according to the procedure described above. They were then autoclaved for 15 min in 0.01 M citric acid buffer (pH 6.8) to activate the antigen. After two 5-min incubations in PBS-Tween20, the sections were incubated at room temperature with anti phosphorylated tau (AT8) or $A\beta_{1-42}$ primary antibody (BC05) overnight. After three 2-min incubations in PBS-Tween20, they were incubated with biotinylated goat anti-mouse IgG at room temperature for 1 h. After three 5-min. incubations in PBS-Tween20, the sections were incubated with Streptavidin–Peroxidase complex at room temperature for 30 min. After three 2-min incubations in PBS-Tween20, they were incubated with DAB as a chromogen for 30 min. After being washed with water, the sections were observed under a microscope.

4.7. Fluorescent staining of AD brain sections

Postmortem brain tissues from an autopsy-confirmed case of AD (a 93-year-old, female) were obtained from the Graduate School of Medicine, Kyoto University. Deparaffinization was carried out according to the procedure described above. The brain tissue was incubated with a 50% ethanol solution (300 μM) of **2c** (**SBIM-3**) for 30 min. Finally, the section was washed in ethanol for 30 s. Fluorescent observation was performed with the Keyence system (excitation filter, 450–490 nm; emission filter, 510–560 nm; DM filter; 495 nm). The same patient's brain section was stained with ThS, a pathological dye used for staining NFT in the brain, and observed with the Keyence system (excitation filter, 450–490 nm; emission filter, 510–560 nm; DM filter; 495 nm).

This experiment was performed under a fluorescence microscope (BIOREVO BZ-9000, Keyence Corp., Osaka, Japan).

4.8. In vivo biodistribution in normal mice

The experiments with animals were conducted in accordance with our institutional guidelines and approved by the Kyoto University. A saline solution (100 μL) of [^{125}I]**2a** ([^{125}I]**SBIM-1**), [^{125}I]**2b** ([^{125}I]**SBIM-2**), and [^{125}I]**2c** ([^{125}I]**SBIM-3**) (13.2–20.6 kBq) containing ethanol (10 μL) was injected intravenously directly into the tail of ddY mice (5-week-old, male). The mice were sacrificed at various time points post-injection. The organs of interest were removed and weighed, and the radioactivity was measured with an automatic g counter.

Acknowledgments

This study was supported by the Funding Program for Next Generation World-Leading Researchers and JSPS Research Fellowships for Young Scientists. We thank Professor Hiroshi Mori for kindly providing human tau cDNA for the in vitro binding assays.

References and notes

1. Selkoe, D. J. *Physiol. Rev.* **2001**, *81*, 741.
2. Braak, H.; Braak, E. *Neurobiol. Aging* **1997**, *18*, 351.
3. Thal, D. R.; Rub, U.; Orantes, M.; Braak, H. *Neurology* **2002**, *58*, 1791.
4. Ono, M.; Wilson, A.; Nobrega, J.; Westaway, D.; Verhoeff, P.; Zhuang, Z. P.; Kung, M. P.; Kung, H. F. *Nucl. Med. Biol.* **2003**, *30*, 565.
5. Verhoeff, N. P.; Wilson, A. A.; Takeshita, S.; Trop, L.; Hussey, D.; Singh, K.; Kung, H. F.; Kung, M. P.; Houle, S. *Am. J. Geriatr. Psychiatry* **2004**, *12*, 584.
6. Klunk, W. E.; Engler, H.; Nordberg, A.; Wang, Y.; Blomqvist, G.; Holt, D. P.; Bergstrom, M.; Savitcheva, I.; Huang, G. F.; Estrada, S.; Ausen, B.; Debnath, M. L.; Barletta, J.; Price, J. C.; Sandell, J.; Lopresti, B. J.; Wall, A.; Koivisto, P.; Antoni, G.; Mathis, C. A.; Langstrom, B. *Ann. Neurol.* **2004**, *55*, 306.
7. Mathis, C. A.; Wang, Y.; Holt, D. P.; Huang, G. F.; Debnath, M. L.; Klunk, W. E. *J. Med. Chem.* **2003**, *46*, 2740.
8. Kudo, Y.; Okamura, N.; Furumoto, S.; Tashiro, M.; Furukawa, K.; Maruyama, M.; Itoh, M.; Iwata, R.; Yanai, K.; Arai, H. *J. Nucl. Med.* **2007**, *48*, 553.
9. Shoghi-Jadid, K.; Small, G. W.; Agdeppa, E. D.; Kepe, V.; Ercoli, L. M.; Siddarth, P.; Read, S.; Satyamurthy, N.; Petric, A.; Huang, S. C.; Barrio, J. R. *Am. J. Geriatr. Psychiatry* **2002**, *10*, 24.
10. Agdeppa, E. D.; Kepe, V.; Liu, J.; Flores-Torres, S.; Satyamurthy, N.; Petric, A.; Cole, G. M.; Small, G. W.; Huang, S. C.; Barrio, J. R. *J. Neurosci.* **2001**, *21*, RC189.
11. Zhang, W.; Oya, S.; Kung, M. P.; Hou, C.; Maier, D. L.; Kung, H. F. *Nucl. Med. Biol.* **2005**, *32*, 799.
12. Rowe, C. C.; Ackerman, U.; Browne, W.; Mulligan, R.; Pike, K. L.; O'Keefe, G.; Tochon-Danguy, H.; Chan, G.; Berlangieri, S. U.; Jones, G.; Dickinson-Rowe, K. L.; Kung, H. P.; Zhang, W.; Kung, M. P.; Skovronsky, D.; Dyrks, T.; Holl, G.; Krause, S.; Friebe, M.; Lehman, L.; Lindemann, S.; Dinkelborg, L. M.; Masters, C. L.; Villemagne, V. L. *Lancet Neurol.* **2008**, *7*, 129.
13. Wong, D. F.; Rosenberg, P. B.; Zhou, Y.; Kumar, A.; Raymont, V.; Ravert, H. T.; Dannals, R. F.; Nandi, A.; Brasic, J. R.; Ye, W.; Hilton, J.; Lyketsos, C.; Kung, H. F.; Joshi, A. D.; Skovronsky, D. M.; Pontecorvo, M. J. *J. Nucl. Med.* **2010**, *51*, 913.
14. Choi, S. R.; Golding, G.; Zhuang, Z.; Zhang, W.; Lim, N.; Hefti, F.; Benedum, T. E.; Kilbourn, M. R.; Skovronsky, D.; Kung, H. F. *J. Nucl. Med.* **1887**, *2009*, 50.
15. Newberg, A. B.; Wintering, N. A.; Plossl, K.; Hochold, J.; Stabin, M. G.; Watson, M.; Skovronsky, D.; Clark, C. M.; Kung, M. P.; Kung, H. F. *J. Nucl. Med.* **2006**, *47*, 748.
16. Scheinin, N. M.; Aalto, S.; Koikkalainen, J.; Lotjonen, J.; Karrasch, M.; Kemppainen, N.; Viitanen, M.; Nagren, K.; Helin, S.; Scheinin, M.; Rinne, J. O. *Neurology* **2009**, *73*, 1186.
17. Cummings, J. L. *Neurobiol. Aging* **2010**, *31*, 1481.
18. Gomez-Isla, T.; Hollister, R.; West, H.; Mui, S.; Growdon, J. H.; Petersen, R. C.; Parisi, J. E.; Hyman, B. T. *Ann. Neurol.* **1997**, *41*, 17.
19. Arriagada, P. V.; Growdon, J. H.; Hedley-Whyte, E. T.; Hyman, B. T. *Neurology* **1992**, *42*, 631.
20. Nelson, P. T.; Alafuzoff, I.; Bigio, E. H.; Bouras, C.; Braak, H.; Cairns, N. J.; Castellani, R. J.; Crain, B. J.; Davies, P.; Del Tredici, K.; Duyckaerts, C.; Frosch, M. P.; Haroutunian, V.; Hof, P. R.; Hulette, C. M.; Hyman, B. T.; Iwatsubo, T.; Jellinger, K. A.; Jicha, G. A.; Kovari, E.; Kukull, W. A.; Leverenz, J. B.; Love, S.; Mackenzie, I. R.; Mann, D. M.; Masliah, E.; McKee, A. C.; Montine, T. J.; Morris, J. C.; Schneider, J. A.; Sonnen, J. A.; Thal, D. R.; Trojanowski, J. Q.; Troncoso, J. C.; Wisniewski, T.; Woltjer, R. L.; Beach, T. G. *J. Neuropathol. Exp. Neurol.* **2012**, *71*, 362.
21. Okamura, N.; Suemoto, T.; Furumoto, S.; Suzuki, M.; Shimadzu, H.; Akatsu, H.; Yamamoto, T.; Fujiwara, H.; Nemoto, M.; Maruyama, M.; Arai, H.; Yanai, K.; Sawada, T.; Kudo, Y. *J. Neurosci.* **2005**, *25*, 10857.
22. Fodero-Tavoletti, M. T.; Okamura, N.; Furumoto, S.; Mulligan, R. S.; Connor, A. R.; McLean, C. A.; Cao, D.; Rigopoulos, A.; Cartwright, G. A.; O'Keefe, G.; Gong, S.; Adlard, P. A.; Barnham, K. J.; Rowe, C. C.; Masters, C. L.; Kudo, Y.; Cappai, R.; Yanai, K.; Villemagne, V. L. *Brain* **2011**, *134*, 1089.
23. Ono, M.; Hayashi, S.; Matsumura, K.; Kimura, H.; Okamoto, Y.; Ihara, M.; Takahashi, R.; Mori, H.; Saji, H. *ACS Chem. Neurosci.* **2011**, *2*, 269.
24. Matsumura, K.; Ono, M.; Hayashi, S.; Kimura, H.; Okamoto, Y.; Ihara, M.; Takahashi, R.; Mori, H.; Saji, H. *Med. Chem. Commun.* **2011**, 596.
25. Matsumura, K.; Ono, M.; Kimura, H.; Ueda, M.; Nakamoto, Y.; Togashi, K.; Okamoto, Y.; Ihara, M.; Takahashi, R.; Saji, H. *ACS Med. Chem. Lett.* **2011**, *3*, 58.
26. Zhang, W.; Arteaga, J.; Cashion, D. K.; Chen, G.; Gangadharmath, U.; Gomez, L. F.; Kasi, D.; Lam, C.; Liang, Q.; Liu, C.; Mocharla, V. P.; Mu, F.; Sinha, A.; Szardenings, A. K.; Wang, E.; Walsh, J. C.; Xia, C.; Yu, C.; Zhao, T.; Kolb, H. C. *J. Alzheimers Dis.* **2012**, *31*, 1.
27. Villemagne, V. L.; Furumoto, S.; Fodero-Tavoletti, M. T.; Pejoska, S.; Kudo, Y.; Mulligan, R. S.; Hodges, J.; Masters, C. L.; Yanai, K.; Rowe, C. C.; Okamura, N. Human Amyloid Imaging Conference, 2012.
28. Dishino, D. D.; Welch, M. J.; Kilbourn, M. R.; Raichle, M. E. *J. Nucl. Med.* **1983**, *24*, 1030.
29. Giger, M.; Baumgartner, H. R.; Zbinden, G. *Agents Actions* **1974**, *4*, 173.
30. Han, D.; Qureshi, H. Y.; Lu, Y.; Paudel, H. K. *J. Biol. Chem.* **2009**, *284*, 13422.